IEIE Transactions on Smart Processing and Computing, vol. 5, no. 1, February 2016
http://dx.doi.org/10.5573/IEIESPC.2016.5.1.22

IEIE Transactions on Smart Processing and Computing

Design of a Luenberger Observer–based Current Sensorless Multi-loop Control for Boost Converters

Xutao Li, Minjie Chen, Hirofumi Shinohara, and Tsutomu Yoshihara

Graduate School of Information, Production and Systems, Waseda University / Fukuoka, Japan
yoshiharatsutomu@waseda.jp

***** Corresponding Author: Yoshihara Tsutomu

Received February 15, 2016; Accepted February 24, 2016; Published February 29, 2016

** Extended from a Conference: Preliminary results of this paper were presented at the ICEIC 2016. This paper has been accepted by the editorial board through the regular review process that confirms the original contribution.*

***Abstract*:** Multi-loop control of a boost converter needs a current-sensing circuit to detect the inductor current. Current sensorless multi-loop control reduces the cost, size and weight of the converter. The Luenberger observer (LO) is widely used to estimate the inductor current for current sensorless control of a switching converter. However, the design of the LO-based sensorless multi-loop control has not been well presented, so far. In this paper, a closed-loop characteristics evaluation method is proposed to design an LO-based current sensorless multi-loop control for boost converters. Simulations show evaluations of the closed-loop characteristics. Practical experiments on a digital processor confirm the simulations.

***Keywords*:** Boost converter, Sensorless current control, Luenberger observer, Closed-loop characteristics

1. Introduction

The controller of a switching converter should first guarantee that the power conversion is stable under all operating conditions, and next, that the desired dynamic performance is maintained when a disturbance occurs in the circuit. For a single-loop output voltage controlled buck converter or a boost converter in discontinuous conduction mode, stability and dynamic performance can be guaranteed by making the loop gain as large as possible, with a high crossover frequency and an adequate phase and gain margin [1]. Nevertheless, there is a right-half-plane-zero (RHPZ) [2] in the transfer function from the duty ratio to the output voltage for a boost, a buck-boost and a fly-back converter in continuous conduction mode (CCM). This RHPZ severely restricts the crossover frequency of the loop gain, and results in poor dynamic performance for single-loop voltage control. Multi-loop control is widely adopted to improve dynamic performance [3]. However, multi-loop control needs a current-sensing circuit, such as a shunt resistor with an amplifier, a transformer or an active filter to detect the inductor current [4], which results in an increase in the cost, size and weight of the circuit. Current sensorless multi-loop control solves this problem through an inductor current estimation approach: utilizing the integral of the voltage drop on the inductor to estimate the inductor current was introduced [5, 6], utilizing the predictive inductor current for peak current control was introduced [7, 8], and a state observer was introduced [9, 10]. Investigations show that the Luenberger observer (LO) [11] is easy to understand and effective in estimating the inductor current for sensorless control of a converter.

The dynamic performance of a converter is determined by its closed-loop characteristics, including audio-susceptibility and output impedance [12]. For multi-loop control, the relationships between the loop gains and the closed-loop characteristics are generally indirect [13], and as a result, minimizing the audio-susceptibility and output impedance involves an iterative process. It is more difficult to design an LO-based sensorless multi-loop control for a converter, because there are more parameters relating to closed-loop characteristics. Although the LO-based sensorless control was introduced in previous papers [14, 15], its design has not been well studied. Therefore, in this paper, a closed-loop characteristics evaluation method is proposed to design the LO-based current sensorless multi-

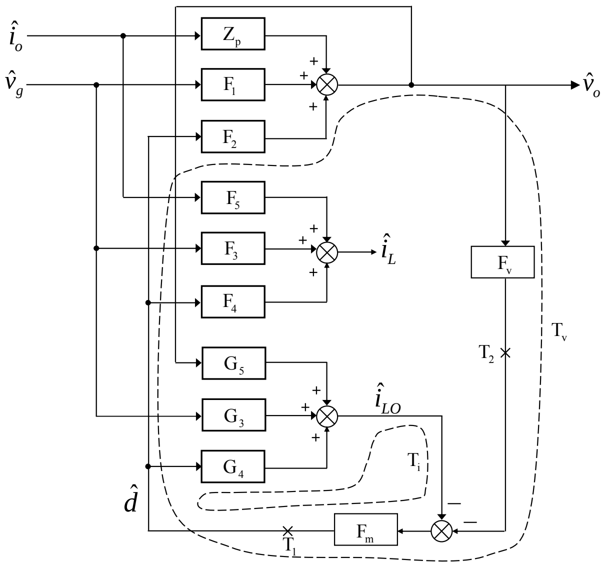

Fig. 1. Block diagram of LO-based sensorless control.

loop control for boost converters in CCM. Simulations show evaluations of the closed-loop characteristics. Practical experiments on a digital processor confirm the simulations.

2. The Proposed Design Method

2.1 Block Diagram of LO-based Control

The topology-independent block diagram for LO-based sensorless multi-loop control of a converter is shown in Fig. 1. The control system consists of an outer loop T_v, and an inner loop T_i. The outer loop provides a reference inductor current for the inner current loop. The symbols $\hat{v}_o$, $\hat{v}_g$, $\hat{i}_o$, and $\hat{i}_L$ are the small signals of the converter. F_1, F_2, F_3, F_4, F_5, and Z_p are the transfer functions of the power stage. F_m and F_v are the inner and outer compensators, respectively. $\hat{i}_{LO}$ is the estimated inductor current by the LO in Eq. (1):

$$\dot{x} = Ax + Bu + L(\hat{v}_o - \hat{v}_{LO}) \tag{1}$$

where $x = [\hat{i}_{LO} \;\; \hat{v}_{LO}]$ is the estimated system state, and u is the observer input. The matrices A, B, and C come from the model of the converter, and L is the parameter of the LO. The transfer functions G_3, G_4, and G_5 can be obtained through Laplace transformation of Eq. (1).

2.2 Closed-loop Stability Evaluation

Denote the current loop gain $T_i = F_mG_4$, and the voltage loop gain $T_v = F_mF_vF_2 + F_mG_5F_2$. The total gain at the point T_1 and the outer gain at the point T_2 are written in Eqs. (2) and (3), respectively. The closed-loop stability can be examined through the open-loop transfer functions given in Eqs. (2) and (3).

$$T_1 = F_mG_4 + F_mF_vF_2 + F_mG_5F_2 \tag{2}$$

$$T_2 = \frac{F_mF_vF_2 + F_mG_5F_2}{1 + F_mG_4} \tag{3}$$

From Eqs. (2) and (3), it is known that the crossover frequency of current loop T_i should be as high as possible to provide a critical 90^0 phase boost for outer loop T_v, while its loop gain should be as small as possible at low frequencies. Loop gain T_v should be as large as possible to attenuate the disturbance on the output voltage.

2.3 Closed-loop Performance Evaluation

Dynamic performance of a converter is determined by its closed-loop dynamic characteristics. From Fig. 1, the closed-loop audio-susceptibility and the output impedance of output voltage are given in Eqs. (4) and (5), respectively.

$$\frac{\hat{v}_o(s)}{\hat{v}_g(s)} = \frac{F_1 + F_m(F_1G_4 - F_2G_3)}{1 + F_mG_4 + F_mF_vF_2 + F_mG_5F_2} \tag{4}$$

$$\frac{\hat{v}_o(s)}{\hat{i}_o(s)} = \frac{Z_p + F_mZ_pG_4}{1 + F_mG_4 + F_mF_vF_2 + F_mG_5F_2} \tag{5}$$

The dynamic performance of inductor current $\hat{i}_L$ can be evaluated by the closed-loop characteristics in Eqs. (6) and (7).

$$\frac{\hat{i}_L(s)}{\hat{v}_g(s)} = \frac{F_3(1 + F_mG_4) + F_m[(F_2F_3 - F_1F_4)(F_v + G_5) - F_4G_3]}{1 + F_mG_4 + F_mF_vF_2 + F_mG_5F_2} \tag{6}$$

$$\frac{\hat{i}_L(s)}{\hat{i}_o(s)} = \frac{F_5(1 + F_mG_4) + F_m(F_2F_5 - F_4Z_p)(F_v + G_5)}{1 + F_mG_4 + F_mF_vF_2 + F_mG_5F_2} \tag{7}$$

Similarly, dynamic performance of estimated inductor current $\hat{i}_{LO}$ can also be evaluated by the closed-loop characteristics in Eqs. (8) and (9).

$$\frac{\hat{i}_{LO}(s)}{\hat{v}_g(s)} = \frac{G_3 + F_mF_v(F_2G_3 - F_1G_4) + F_1G_5}{1 + F_mG_4 + F_mF_vF_2 + F_mG_5F_2} \tag{8}$$

$$\frac{\hat{i}_{LO}(s)}{\hat{i}_o(s)} = \frac{-F_mF_vG_4Z_p + Z_pG_5}{1 + F_mG_4 + F_mF_vF_2 + F_mG_5F_2} \tag{9}$$

3. Design of LO-based Sensorless Multi-loop Control for Boost Converters

3.1 Small Signal Average Value Model

The boost converter used in this paper is shown in Fig. 2, in which several parasitic components are considered. Its small signal average value model in CCM is written in Eq. (10):

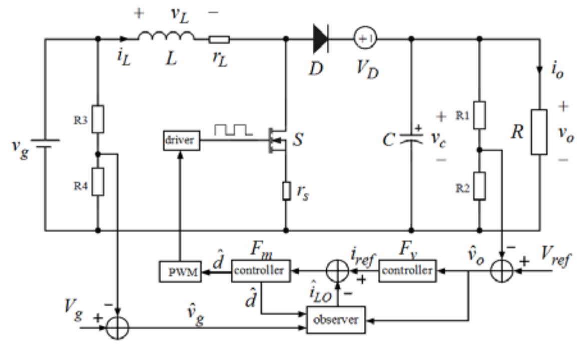

Fig. 2. LO-based control of a boost converter.

$$\dot{x} = Ax + B\hat{d} + Ew \tag{10}$$

where $x = [\hat{i_L}\ \ \hat{v_c}]$, $w = [\hat{v_g}\ \ \hat{i_o}]$, and

$$A = \begin{bmatrix} -\dfrac{r_L + Dr_s}{L} & -\dfrac{D'}{L} \\ \dfrac{D'}{C} & -\dfrac{1}{RC} \end{bmatrix},\quad E = \begin{bmatrix} \dfrac{1}{L} & 0 \\ 0 & -\dfrac{1}{C} \end{bmatrix}$$

$$B = \begin{bmatrix} \dfrac{(D'R - r_s)V_g + (r_s + r_L)V_D}{L(r_L + Dr_s + D'^2 R)} \\ -\dfrac{V_g - D'V_D}{C(r_L + Dr_s + D'^2 R)} \end{bmatrix}$$

$$D' = \frac{r_s V_{ref} + RV_g}{2R(V_{ref} + V_D)}\left(1 + \sqrt{1 - \frac{4R(r_L + r_s)(V_{ref} + V_D)V_{ref}}{(r_s V_{ref} + RV_g)^2}}\right)$$

The symbols $\hat{i_L}$, $\hat{v_c}$, $\hat{v_g}$, $\hat{i_o}$, and $\hat{d}$ are the small signals, and $\hat{v_g}$ and $\hat{i_o}$ are the disturbances. The symbol D denotes the duty ratio at a given operating point, $D' = 1-D$, and $\hat{d}$ is the duty ratio adjustment from the given operation point. Ignoring the equivalent series resistance of the output capacitor, $\hat{v_c}$ is equivalent to $\hat{v_o}$. For convenience, define

$$A = \begin{bmatrix} a_{11} & a_{12} \\ a_{21} & a_{22} \end{bmatrix},\quad B = \begin{bmatrix} b_1 \\ b_2 \end{bmatrix},\quad E = \begin{bmatrix} e_1 & 0 \\ 0 & e_2 \end{bmatrix}$$

3.2 Transfer Functions in Fig. 1

Through Laplace transformation of Eq. (10), the transfer functions F_1, F_2, F_3, F_4, F_5, and Z_p in Fig. 1 are obtained as follows:

$$F_1 = \frac{a_{21}e_1}{\Delta} \tag{11}$$

$$F_2 = \frac{b_2 s + a_{21}b_1 - a_{11}b_2}{\Delta} \tag{12}$$

$$F_3 = \frac{e_1 s - e_1 a_{22}}{\Delta} \tag{13}$$

$$F_4 = \frac{b_1 s + a_{12}b_2 - a_{22}b_1}{\Delta} \tag{14}$$

$$F_5 = \frac{a_{12}e_2}{\Delta} \tag{15}$$

$$Z_p = \frac{e_2 s - a_{11}e_2}{\Delta} \tag{16}$$

where $\Delta = s^2 - (a_{11} + a_{22})s + a_{11}a_{22} - a_{12}a_{21}$. Substituting the matrices A, B, and C in Eq. (10) into Eq. (1) and performing Laplace transformation, the transfer functions G_3, G_4, and G_5 in Fig. 1 are obtained as follows:

$$G_3 = \frac{e_1 s + e_2(a_{12} - l_1) - e_1(a_{22} - l_2)}{\Lambda} \tag{17}$$

$$G_4 = \frac{b_1 s + b_2(a_{12} - l_1) - b_1(a_{22} - l_2)}{\Lambda} \tag{18}$$

$$G_5 = \frac{l_1 s + l_2 a_{12} - l_1 a_{22}}{\Lambda} \tag{19}$$

where $\Lambda = s^2 - (a_{11} + a_{22} - l_2)s + a_{11}a_{22} - a_{12}a_{21} - a_{11}l_2 + a_{21}l_1$, and l_1 and l_2 are the elements of L in Eq. (1). The PI controllers in Eqs. (20) and (21) are used in Fig. 1 as compensators F_m and F_v, respectively.

$$F_m = K_{Pm} + K_{Im}\frac{1}{s} \tag{20}$$

$$F_v = K_{Pv} + K_{Iv}\frac{1}{s} \tag{21}$$

Let $C = [0\ \ 1]$. The LO in Eq. (1) is written in Eq. (22).

$$\dot{\hat{x}} = \begin{bmatrix} a_{11} & a_{12} \\ a_{21} & a_{22} \end{bmatrix}\hat{x} + \begin{bmatrix} b_1 & e_1 \\ b_2 & 0 \end{bmatrix}u + \begin{bmatrix} l_1 \\ l_2 \end{bmatrix}(v_o - \hat{v}_o) \tag{22}$$

where $\hat{x} = [\hat{i_{LO}}\ \ \hat{v_{LO}}]$ is the estimated system state, and $u = [\hat{d}\ \ \hat{v_g}]$ is the observer input. The controllers in Eqs. (20) and (21), and the LO in Eq. (22), can be designed by the closed-loop evaluations given in Eqs. (2)-(7), and (8).

4. Simulations and Experiments

A boost converter with the parameters listed in Table 1 is used to show the design of the LO-based sensorless current multi-loop control.

Table 1. Parameters of a Boost Converter.

Parameters	Values
Input voltage	v_g = 10 V
Output voltage	v_o = 20 V
Output capacitor	C = 1000 μF
Inductor	L = 47μH , r_L = 24 mΩ
Load	R = 25 mΩ
Switch S	r_s = 36 mΩ
Diode D	v_D = 1.25 V
Switching frequency	f_s = 150 kHz

4.1 Simulations of Closed-loop Stability and Characteristics

First, determine parameter L of the LO in Eq. (22) by eigenvalue assignment $A–LC$. After an iterative process, the eigenvalues $\{-0.0093, -7.5003\}\times10^5$ are found to be suitable, and correspondingly, $L = [0.01\ 0.75]^T\times10^6$. Next, determine the parameters of compensators F_m and F_v in Eqs. (20) and (21). As presented in Section 2, the crossover frequency of the current loop $T_i = F_mG_4$ should be as high as possible to provide a 90^0 phase boost for the outer loop $T_v = F_mF_vF_2 + F_mG_5F_2$, while its loop gain should be as small as possible. Loop gain T_v should be as large as possible to attenuate the disturbance on the output voltage. After an iterative process, $F_m = 0.2 + 250/s$ and $F_v = 30 + 18000/s$ are found to be suitable. The bode plots of T_1 and T_2 in Fig. 1 are given in Fig. 3. Gain T_1 has a crossover frequency of 12.9 kHz, which is about 1/11.6 of switching frequency f_s, with a phase margin of 78.8°. Gain T_2 has a crossover frequency of 2.3 kHz, which is about 1/5.7 of T_1, with a phase margin of 73.5° and a gain margin 18.8 dB. It can be said that the LO in Eq. (22) and the compensators in Eqs. (20) and (21) are well designed, and a stable control system is guaranteed.

The closed-loop characteristics of the output voltage, the inductor current, and the estimated inductor current are shown in Figs. 4, 5 and 6, respectively.

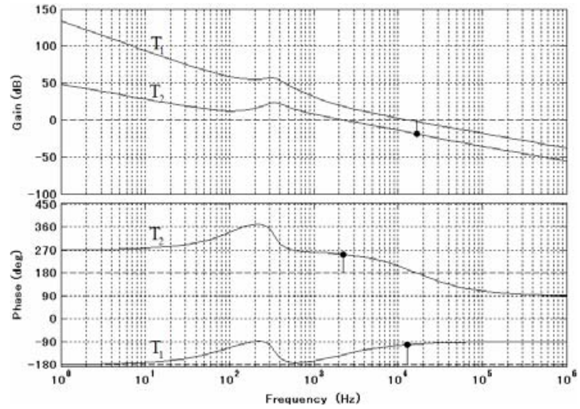

Fig. 3. Bode plots of T_1 and T_2.

The step responses for output voltage are shown in Fig. 7. The step responses of inductor current $\hat{i_L}$ and the estimated inductor current $\hat{i_{LO}}$ are shown in Fig. 8. It shows that the estimated inductor current perfectly estimates the inductor current when the input voltage is disturbed, while

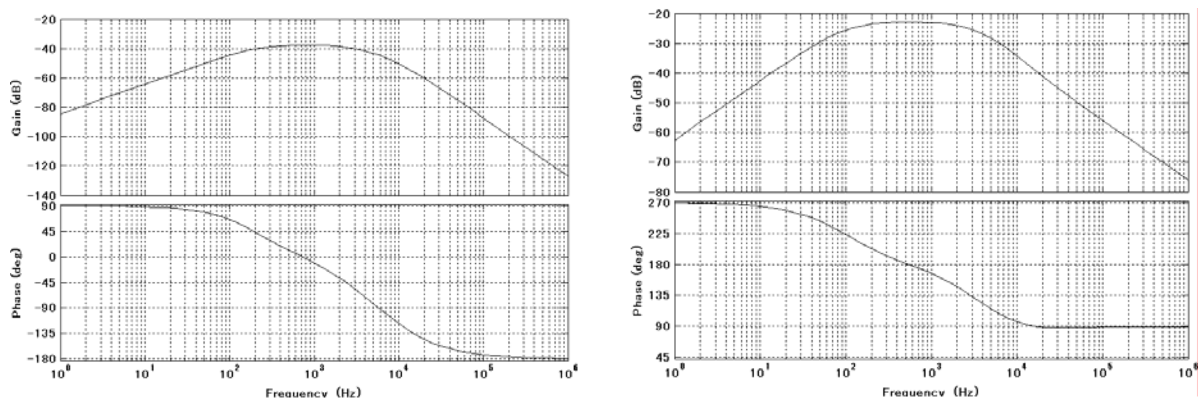

(a) Audio-susceptibility **(b) Output impedance**

Fig. 4. Closed-loop characteristics ($\hat{v_o}$).

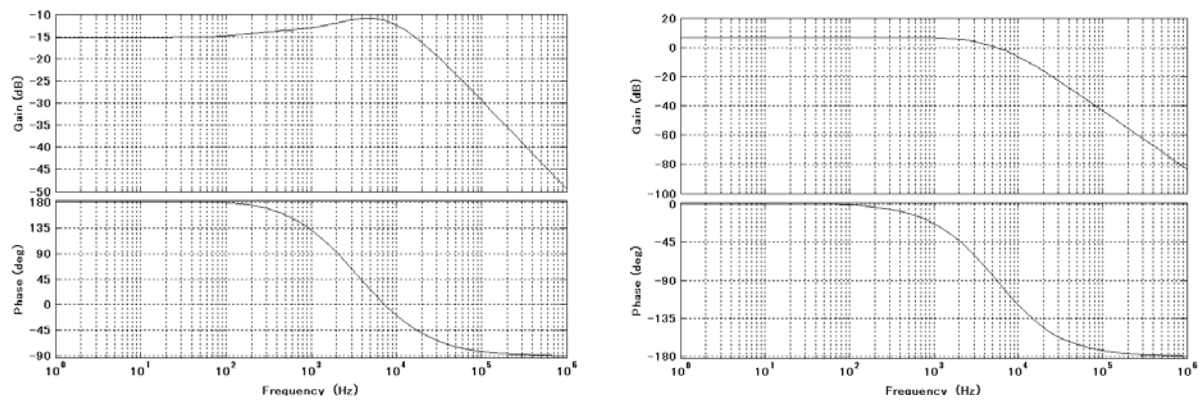

(a) Audio-susceptibility **(b) Output impedance**

Fig. 5. Closed-loop characteristics ($\hat{i_L}$).

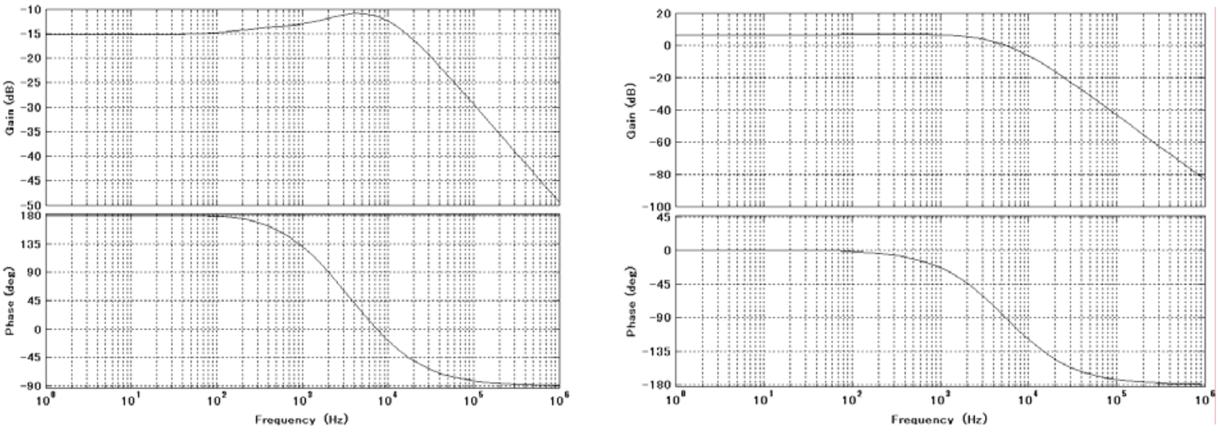

(a) Audio-susceptibility **(b) Output impedance**

Fig. 6. Closed-loop characteristics ($\hat{i_{LO}}$).

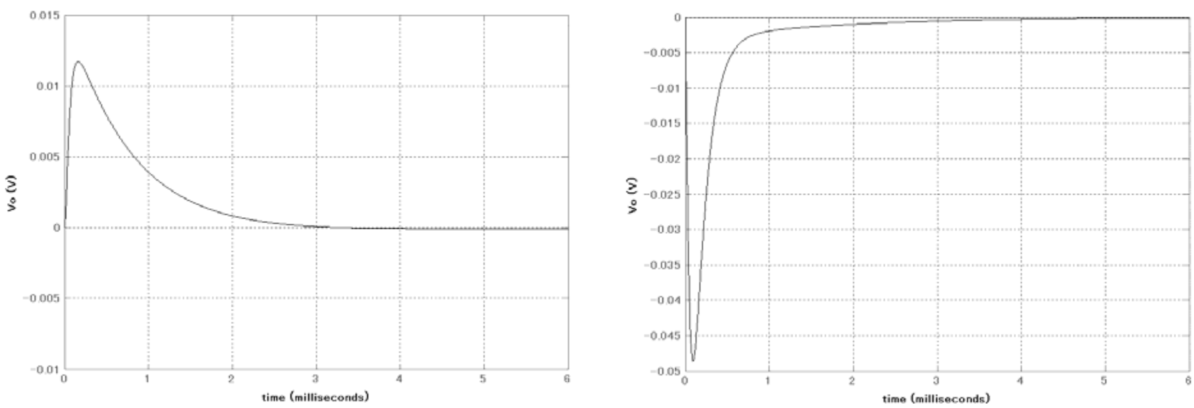

(a) Step response of $\hat{v_o}$ to a step change in $\hat{v_g}$ **(b) Step response of $\hat{v_o}$ to a step change in $\hat{i_o}$**

Fig. 7. Step response of $\hat{v_o}$.

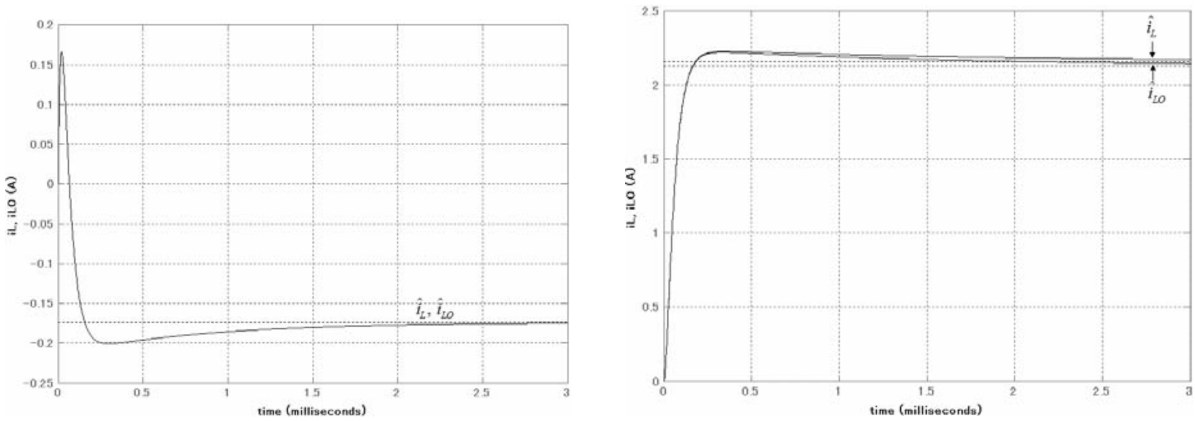

(a) Step responses of $\hat{i_L}$ and $\hat{i_{LO}}$ to a step change in $\hat{v_g}$ **(b) Step responses of $\hat{i_L}$ and $\hat{i_{LO}}$ to a step change in $\hat{i_o}$**

Fig. 8. Step responses of $\hat{i_L}$ and $\hat{i_{LO}}$.

there is a slight error between $\hat{i_L}$ and $\hat{i_{LO}}$ when the load current is disturbed.

4.2 Practical Experiments

The LO and controllers need to be discretized to execute on a digital processor. The discrete counterpart of Eq. (22) is obtained in Eq. (23) by zero-hold discretization.

$$\begin{bmatrix} \hat{i}_{LO}(k+1) \\ \hat{v}_{LO}(k+1) \end{bmatrix} = A \begin{bmatrix} \hat{i}_{LO}(k) \\ \hat{v}_{LO}(k) \end{bmatrix} + B \begin{bmatrix} \hat{d}(k) \\ \hat{v}_g(k) \end{bmatrix} + L\Delta\hat{v}_o(k) \qquad (23)$$

where $\Delta \hat{v_O}(k) = \hat{v_O}(k) - \hat{v_{LO}}(k)$, and

$$A = \begin{bmatrix} 0.9938 & -0.0660 \\ 0.0031 & -0.9996 \end{bmatrix}, \quad B = \begin{bmatrix} 2.9965 & 0.1414 \\ -0.0067 & 0.0002 \end{bmatrix},$$

$$L = \begin{bmatrix} -0.0988 \\ 4.9993 \end{bmatrix}$$

The discrete counterparts of Eqs. (20) and (21) are obtained in Eqs. (24) and (25), respectively, by the backward difference $s = 1 - z^{-1}/T_s$, where T_s is the switching period.

$$F_m = 0.2 + 0.0017(1 - z^{-1}) \tag{24}$$

$$F_v = 30 + 0.1200(1 - z^{-1}) \tag{25}$$

An NJU20010 digital processor produced by New Japan Radio Corp. is used to execute the above discrete LO and controllers. The limit of the duty ratio is set to 0.05~0.88. The slew rates of the load and the input voltage are 250mA/µs and 2.0V/µs, respectively. The practical dynamic responses are shown in Fig. 9.

The experimental environment is shown in Fig. 10.

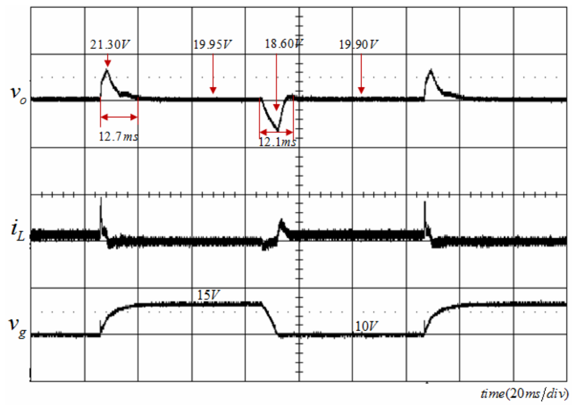

(a) Dynamic response of $\hat{v_o}$ to a disturbance in $\hat{v_g}$

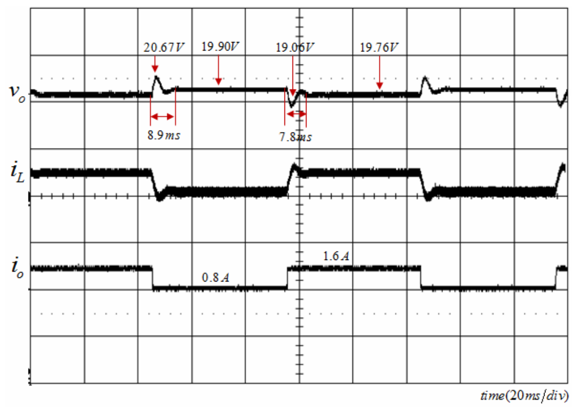

(b) Dynamic response of $\hat{v_o}$ to a disturbance in $\hat{i_o}$

Fig. 9. Practical dynamic responses of $\hat{v_o}$.

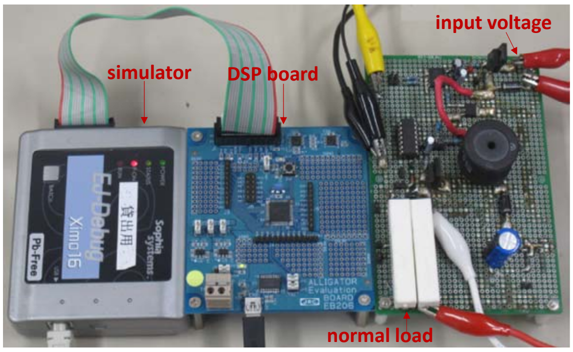

Fig. 10. Experimental environment.

5. Conclusion

The LO can be used to estimate the inductor current for sensorless control of a converter. A closed-loop evaluation method is proposed to design an LO-based sensorless current multi-loop control for boost converters, with a design process as follows: select the parameters of the LO; design the controllers; evaluate closed-loop stability; evaluate the closed-loop characteristics; repeat the above design process until the desired dynamic performance is achieved.

References

[1] X. Li, M. Chen, H. Shinohara, and T. Yoshihara, "Design of an auto-tunable PID controller for buck converters through a robust H∞ synthesis approach," *IEICE Communication Express*, Vol. 5, No. 1, pp. 7-12, Jan. 2016. Article (CrossRef Link)

[2] H. Choi, "Practical feedback loop design considerations for switched mode power supplies," Fairchild semiconductor power seminar, pp. 489-498, 2010-2011. Article (CrossRef Link)

[3] Y. Li, K. R. Vannorsdel, A. J. Zirger, M. Norris, and D. Maksimovic, "Current mode control for boost converters with constant power loads," *IEEE Transactions on Circuits and Systems*, Vol. 59, No. 1, pp. 198-206, Jan. 2012. Article (CrossRef Link) Article (CrossRef Link)

[4] H.P. Forghanizadeh, G.A. Rincon-Mora, "Current-sensing techniques for DC-DC converters," Midwest Symposium on Circuits and Systems, pp. 577-580, Aug. 2002. Article (CrossRef Link)

[5] P. Midya, P. T. Krein, and M. F. Greuel, "Sensorless current mode control—an observer-based technique for DC–DC converters," *IEEE Transactions on Power Electronics*, Vol. 16, No. 4, pp. 522-526, Jul. 2001. Article (CrossRef Link)

[6] J.T. Mossoba, P.T. Krein, "Design and control of sensorless current mode dc-dc converters," *Applied Power Electronics Conference and Exposition*, Vol. 1, pp 315-321, Feb. 2003. Article (CrossRef Link)

[7] Q. Tong, Q. Zhang, R. Min, X. Zou, Z. Liu, and Z. Chen, "Sensorless predictive peak current control for

boost converter using comprehensive compensation strategy," *IEEE Transactions on Industrial Elec tronics*, Vol. 61, No. 6, pp. 2754-2766, June 2013. Article (CrossRef Link)
[8] A. Kelly, K. Rinne, "Sensorless current-mode control of a digital dead-beat DC-DC converter," *Applied Power Electronics Conference and Exposition*, Vol. 3, pp. 1790-1795, Feb. 2004. Article (CrossRef Link)
[9] G. Cimini, G. Ippoliti, G. Orlando, and M. Pirro, "Current sensorless solution for PFC boost converter operating both in DCM and CCM," *Control & Automation (MED)*, pp. 137-142, Jun. 2013. Article (CrossRef Link)
[10] P. Majid, D. Pritam, M. Gerry, J. Praveen, "Sensor-less control of a boost PFC AC/DC Converter with a very fast transient response," *Applied Power Electronics Conference and Exposition (APEC)*, pp. 356-360, Mar. 2013. Article (CrossRef Link)
[11] D. G. Luenberger, "An introduction to observers," *IEEE Transactions on Automatic Control*, Vol. 16, No. 6, pp. 596-602, Dec. 1971. Article (CrossRef Link)
[12] R. Ahmadi, D. Paschedag, M. Ferdowsi, "Closed-loop input and output impedances of dc-dc switching converters operating in voltage and current mode control," *Annual Conference on IEEE Industrial Electronics Society*, pp. 2311-2316, Nov. 2010. Article (CrossRef Link)
[13] R. B. Ridley, B. H. Cho, F. C. Y. LEE, "An analysis and interpretation of loop gains of multi-loop controlled switching regulators," *IEEE Transactions on Power Electronics*, Vol. 3, No. 4, pp. 489-498, Oct. 1988. Article (CrossRef Link)
[14] H. Cho, S. J. Yoo, S. Kwak, "State observer based sensorless control using Lyapunov's method for boost converters". *IET Power Electronics*, Vol. 8, No. 1, pp 11-19, May 2014. Article (CrossRef Link)
[15] V. Spinu, M. Dam, and M. Lazar, "Observer design for dc/dc power converters with bilinear averaged model," *Proceedings of the 4th IFAC Conference on Analysis and Design of Hybrid Systems*, pp. 204-209, Jun. 2012. Article (CrossRef Link)

Xutao Li received his BSc in automation from Wuhan Technology University, China, in 1999, and an MSc in precise instruments and machinery from Shanghai Jiaotong University, China, in 2006. After working for several years in Japan, he is now a Ph.D. candidate in the Graduate School of Information, Production and Systems, Waseda University, Japan. His research interests include switching mode power suppliers and control theory.

Minjie Chen received a BSc in electrical engineering and automation from Shanghai Jiaotong University, China, in 2009, and an MSc from the Graduate School of Information, Production and Systems, Waseda University, Japan. He is now a Ph.D. candidate at Waseda University. His research interest is power converter technology.

Hirofumi Shinohara received a BSc and an MSc in electrical engineering and a Ph.D. in informatics from Kyoto University in 1976, 1978, and 2008, respectively. He has been engaged in administration of collaborative research into VLSI circuits between industry and the semiconductor technology research academic center (STRAC). He is now a professor in the Graduate School of Information, Production and Systems, Waseda University, Japan. His research interests include advanced SRAM, low-power circuits, and variation-aware design.

Tsutomu Yoshihara received his BSc and MSc in physics and a Ph.D. in electronic engineering from Osaka University, Osaka, Japan, in 1969, 1971, and 1983, respectively. In 1971, he joined the ULSI laboratory of Mitsubishi Electric Corp., Hyogo, Japan, where he has been engaged in the research and development of MOS LSI memory. Since April 2003, he has been a Professor in the Graduate School of Information, Production and Systems, Waseda University, Japan, and is currently involved in research on system LSI. He is a member of IEEE Solid-State Circuits, IEICE of Japan, and the Institute of Electrical Engineers of Japan.